# Life extending controller design for reusable rocket engines

**A. Ray and M. S. Holmes**
Mechanical Engineering Department
The Pennsylvania State University, USA

**C. F. Lorenzo**
Instrumentation and Control Division
NASA Glenn Research Center
Cleveland, USA

## ABSTRACT

The goal of life extending control (LEC) is to enhance structural durability of complex mechanical systems, such as aircraft, spacecraft, and energy conversion devices, without incurring any significant loss of performance. This paper presents a concept of robust life-extending controller design for reusable rocket engines, similar to the Space Shuttle Main Engine (SSME), via damage mitigation in both fuel and oxidiser turbines while achieving the required performance for transient responses of the main combustion chamber pressure and the oxidant/fuel mixture ratio. The design procedure makes use of a combination of linear robust control synthesis and nonlinear optimisation techniques. Results of simulation experiments on the model of a reusable rocket engine are presented to this effect.

## 1.0 INTRODUCTION

A reusable rocket engine has a number of critical components that operate close to their mechanical design limits. A major task in the control and operation of reusable rocket engines is to achieve trade-off between dynamic performance and structural durability of critical components. These components often typify behaviour of the remaining components and hence are indicators of the effective service life of the engine. For example, critical components of the SSME that are subjected to a variety of damage modes (e.g., thermo-mechanical fatigue and creep) and potentially limit its service life include the following:

- Blades of the fuel ($H_2$) and oxidiser ($O_2$) turbines
- Combustion chamber and nozzle wall
- Injector tubes

Fatigue damage in injector tubes used to be a source of structural degradation in the SSME. However, this problem has been solved by appropriate selection of materials in the later versions of the SSME. Tensile rupture of the coolant channel ligaments in the combustion chamber and rocket nozzle is primarily caused by creep and creep ratcheting due to the plasticity of copper (and copper alloys) at high temperatures (for example, ~670K). Fatigue damage in fuel and oxidiser turbine blades, which is primarily caused by stress cycling during start-up and shutdown operations of a rocket engine, remains as one of the most serious causes for rocket engine failure.

This paper presents a concept of robust life-extending controller design for reusable rocket engines, similar to the SSME, focusing on damage mitigation in both the fuel and oxidiser turbines while achieving the required performance for transient responses of the combustion chamber pressure and the oxidant/fuel mixture ratio. The concept of LEC design approach presented in this paper is different from the previously reported work in the sense that this approach allows adaptation of the LEC feature to augment a conventional performance controller of a rocket engine. Unlike the previously reported design approaches[1], the proposed technique does not require an optimal feedforward control sequence that is sensitive to plant modelling uncertainties and variations in the initial conditions. Furthermore, for other control applications, such as military aircraft[2] the life extension feature of the control system can be activated or deactivated at the operator's decision.

The paper is organised in five sections including the introduction. Section 2 briefly presents a functional description of the reusable rocket engine under consideration. Section 3 presents an architecture of the life extending control system including the robust linear controller, a continuous-time model of fatigue damage, and the nonlinear damage controller. Section 4 discusses the results of rocket engine simulation including those of engine performance and fatigue damage in the critical components. Section 5 summarises and concludes the paper with recommendations for future work.

## 2.0 DESCRIPTION OF THE REUSABLE ROCKET ENGINE

The reusable rocket engine under consideration is similar to the SSME. A functional diagram for operation and control of the rocket engine under consideration is presented in Fig. 1. The propellants, namely, cryogenic hydrogen ($H_2$) fuel and cryogenic oxygen ($O_2$), are individually pressurised by separate closed cycle turbopumps. Pressurised cryogenic fuel and oxygen are pumped into two high-

**Paper No. 2583.** Manuscript received 26 September 2000, revised version received 1 March 2001, accepted 9 March 2001.

pressure preburners which feed the respective turbines with fuel-rich hot gas. The fuel and oxidiser turbopump speeds and hence the propellant flow into the main thrust are controlled by the respective preburner. The exhaust from each turbine is injected into the main combustion chamber where it burns with the oxidiser to make the most efficient use of the energy. The oxygen flow into each of the two preburners is independently controlled by the respective servo-valves while the valve position for oxygen flow into the main thrust chamber is held in a fixed position to derive the maximum possible power from the engine. The plant outputs of interest are the $O_2/H_2$ mixture ratio the and main thrust chamber pressure which are closely related to the rocket engine performance in terms of specific impulse, thrust-to-weight ratio, and combustion temperature.

A thermo-fluid-dynamic model of the rocket engine has been formulated for plant performance analysis and control systems synthesis[3]. Standard lumped parameter methods have been used to approximate the partial differential equations describing mass, momentum, and energy conservation by a set of first-order differential equations. The plant model is constructed by causal interconnection of the primary subsystem models such as main thrust chamber, preburners, turbopumps, fuel and oxidiser supply header, and fixed nozzle regeneration cooling. The plant model has 20 state variables, two control inputs, and two controlled outputs.

## 3.0 LIFE-EXTENDING CONTROL SYSTEM ARCHITECTURE

The concept of life extending control (LEC) was introduced by Lorenzo and Merrill[4] and Ray *et al*[5]. Subsequently, a growing body of literature has emerged for feedforward and feedback control of rocket engines[1,6]. While the LEC technology was originally developed for rocket engines, it has also found broad applications in other aerospace and mechanical systems such as rotorcraft[7,8], aircraft structures[2], and fossil power plants[9,10]. Efficacy of the LEC concept has also been demonstrated by laboratory experimentation on a test apparatus[11].

Figure 2 shows the architecture of the two-tier life-extending control LEC system. The performance controller in the inner loop is designed to achieve a high level of dynamic performance. In the typical situation with a linearised model of the plant (i.e. rocket

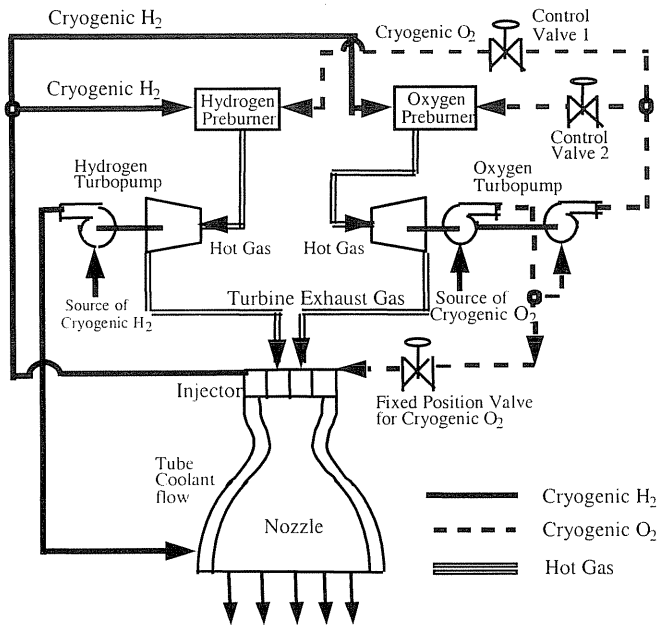


Figure 1. Functional diagram of the reusable rocket engine.

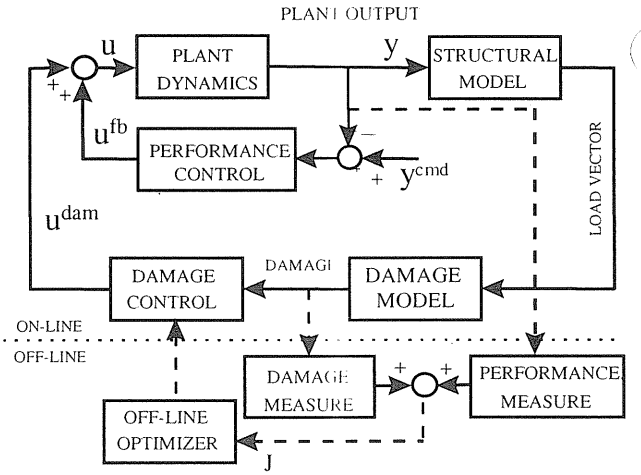


Figure 2. Schematic diagram of life-extending control system and off-line optimiser.

engine) dynamics, this controller can be designed using linear control synthesis techniques such as $H_\infty$-based $\mu$-synthesis to assure stability and performance robustness. The combination of plant dynamics and the performance controller in the inner loop becomes the augmented plant for the nonlinear damage controller design in the outer loop (see Fig. 2). The essential elements of the damage controller in the outer loop are:

- The structural model that uses appropriate plant outputs to estimate the load conditions (e.g. stress at the critical locations);
- The time-domain model of fatigue crack damage that uses the load conditions to determine the (thermomechanical) fatig damage rate and accumulation at the critical structures (e.g. tu bine blades);
- The damage controller which is designed to reduce the damage rate and accumulation at the critical points, specifically under transient operations where the time-dependent load on the stressed structure is controllable.

salient features of this controller design approach are: (*i*) The inner loop controller is designed independently of the outer loop controller by standard commercially available software (e.g. MATLAB); (*ii*) It is not necessary to determine an optimal feedforward control sequence which is sensitive to plant modelling uncertainties and variations in the initial conditions; and (*iii*) for some control applications, such as military aircraft, the damage controller in the outer loop can be activated or deactivated at the the discretion of a human operator or decision module at a higher level in the hierarchy.

### 3.1 Linear Robust Performance Controller in the Inner Loop

This sub-section presents the design of a sampled-data performance controller for the reusable rocket engine by using the (linear) $H_\infty$ (or induced $L_2$ norm to $L_2$ norm) controller synthesis technique[12]. This controller design method minimises the worst case gain between the energy of the exogenous inputs and the energy of the regulated outputs of a generalised plant as presented below.

Bamieh and Pearson[13] proposed a solution to the induced $L_2$ norm controller synthesis problem for application to sampled-data systems. This design procedure has subsequently been incorporat following Sivashankar and Khargonekar[14] as the function *sdhf* in the MATLAB *mutools* toolbox[15] to demonstrate feasibility of the damage mitigation architecture proposed in Fig. 2. In this application, the performance controller needs to have very good disturbance rejection capabilities in the low-frequency range to prevent the damage controller output, $u^{dam}$, from causing a long settling time in the

rocket engine outputs. For other applications, the linear controller in the inner loop of Fig. 2 could be designed with different performance objectives.

Figure 3 shows the setup used for synthesis of the induced $L_2$ norm controller for rocket engine operations based on a linearised plant model with two inputs (fuel preburner oxidiser valve position and oxidiser preburner oxidiser valve position) and two outputs (main thrust chamber hot-gas pressure and $O_2/H_2$ mixture ratio). The plant model is obtained by first linearising the 20-state nonlinear model of the rocket engine at a combustion pressure of 2,550psi (17·58MPa) and an $O_2/H_2$ ratio of 6·02. The pressure 2,550psi (17·58MPa) is chosen for linearisation because the controller is required to operate in the range 2,100psi (14·48MPa) to 3,000psi (20·69MPa). After linearisation, the 20-state linear model is reduced to a 15-state linear model for the controller design via Hankel model order reduction[12]. A comparison of Bode plots reveals that reducing the 20-state model to 15 states does not significantly alter the input-output characteristics of the original model. Since the induced $L_2$-norm controller synthesis procedure being used here requires a strictly proper generalised plant model, the problem of a non-zero D-matrix is circumvented by filtering the outputs of the controller by a first order filter with a very high frequency pole that is selected to be $10^4$rad/sec in this paper:

$$W_{filter}(s) = \frac{10^4}{s+10^4} \quad \ldots (1)$$

The input multiplicative configuration is chosen to represent the plant model uncertainties due to parametric errors and unmodelled high frequency dynamics. The sampler and zero order hold associated with the controller are implicit in the setup used for robust stability where each of the two components of the frequency-dependent disturbance weight $W_{del}$ is chosen to be

$$W_{del}(s) = \frac{s+1}{s+10} \quad \ldots (2)$$

which implies that the amount of plant uncertainty is estimated as being approximately 10% at low frequencies and 100% at high frequencies. The uncertainty model is constructed based on the assumptions of the rocket engine design and operation and can be updated as additional analytical or experimental data become available. Since the plant model is validated with steady-state design data, it is more accurate in the low frequency range. The plant model is a finite-dimensional lumped-parameter representation that may not capture the dynamics of high frequency modes. This leads to the presence of a larger amount of uncertainty in the high frequency region of the model as compared to the uncertainty at low frequencies.

The frequency-dependent performance weight, $W_{perf}$, consists of two components: (*i*) $W_{press}$, which penalises the tracking error of combustion chamber pressure and (*ii*) $W_{O_2/H_2}$, which penalises the tracking error of the $O_2/H_2$ ratio. The frequency-dependent control signal weight, $W_{cont}$, consists of two components: (*i*) $W_{H_2}$ to penalise the fuel preburner oxidiser valve motion and (*ii*) $W_{O_2}$ to penalise the oxidiser preburner oxidiser valve motion. The objectives of these frequency-dependent weights are: (*i*) prevention of large oscillations in the feedback control signal to avoid valve saturation; and (*ii*) reduction of valve wear and tear due to high-frequency movements.

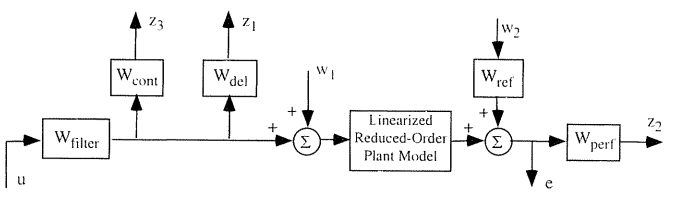


Figure 3. Generalised plant for robust linear controller synthesis.

The parameters of both performance weights and control weights are initially selected based on the control system performance requirements and the knowledge of the plant dynamics. Subsequently, these parameters are fine-tuned using the time-domain responses of the simulation experiments. For this rocket engine controller design, the performance weights are:

$$W_{press}(s) = \frac{4(s+1.75)}{s+1}$$
$$W_{O_2/H_2}(s) = \frac{4000(s+0.5)}{s+0.1} \quad \ldots (3)$$

based on the requirements of the desired rocket engine behaviour in the closed loop. Notice that the chamber pressure transients are more heavily penalised in the low frequency range up to 1rad/sec than at relatively higher frequency range of 1·75rad/sec and above. In contrast, the $O_2/H_2$ mixture ratio that affects engine efficiency is penalised in the low frequency range up to 0·1rad/sec than at relatively higher frequency range of 0·5rad/sec and above. The identical control weights for both $O_2$ and $H_2$ preburner valves are specified as:

$$W_{H_2}(s) = \frac{1200(s+0.75)}{s+10};$$
$$W_{O_2}(s) = \frac{1200(s+0.75)}{s+10} \quad \ldots (4)$$

Notice that the control efforts are penalised in the bandwidth of 0·75 to 10rad/sec to prevent potential oscillations of the actuators in this frequency range. Each of the two components of the frequency-dependent reference signal weight in Fig. 3, $W_{ref}$, which serve as shaping filters, is chosen to be:

$$W_{ref}(s) = \frac{0.5}{s+0.5} \quad \ldots (5)$$

Using the generalised plant model in Fig. 3, a sampled-data controller is designed which is optimal in the sense of induced $L_2$-norm. As guaranteed by the design method employed, the controller has 25 states, which is the same as the number of states in the generalised plant model consisting of the reduced order plant model (15 states), the uncertainty model (2 states), the control signal filters (2 states), the performance weighting matrix (2 states), the reference signal weighting matrix (2 states), and the control signal weighting matrix (2 states). The controller provides acceptable reference signal tracking for the plant without expending a large amount of control effort. It is found that reducing the order of the sampled-data controller from 25 states to 15 states causes no significant change in the controller dynamics from an input/output point of view. Consequently, this reduction causes no noticeable difference in the simulation results produced by the 25-state and 15-state controllers. The 15-state controller is used in what follows.

### 3.2 Fatigue damage modelling

A wide variety of damage mechanisms exist in the reusable rocket engine including: (cycle-dependent) thermomechanical fatigue and (time-dependent) high temperature creep. This paper focuses on thermomechanical fatigue damage in the turbine blades. Different aspects of fatigue damage have been reported by many investigators

as cited in research monographs (e.g. Suresh[16]) on fracture mechanics. While the Paris-type fatigue crack growth models (e.g. the FASTRAN model[17]) are suitable for life prediction of (crack-prone) airframe structures, made of polycrystalline aluminum alloys, the crack initiation models (e.g. Coffin-Manson-type strain-life models) are more appropriate for damage prediction in hot sections of engine components (e.g. blades, disks, and vanes) that are usually made of near-perfect materials such as single-crystal and directionally-solidified super-alloys. Furthermore, since the damage model has to be embedded in the LEC loop for real-time operation, it should be mathematically and computationally as simple as possible, while representing the damage characteristics with adequate accuracy for control purposes. The implication is that the knowledge of the damage and damage rate in the absolute sense may not be so important as the mathematical structure of the damage equation. In other words; the relative (nonlinear) behaviour of damage must be captured by an appropriate mathematical expression in the control algorithm. We reiterate that computational simplicity becomes especially important for real-time execution as well as for large-scale nonlinear optimisation in the design procedure. The mathematical structure of the fatigue damage model needs to be reformulated in the continuous-time setting for use in the LEC design procedure and for implementation of the controller itself. This is accomplished following the approach of Ray *et al*[5].

The (uniaxial) fatigue damage model, used in the controller design, assumes that damage occurs only under tensile loading. A simplified model of fatigue damage is extracted from the continuous-time damage models of Ray *et al*[5] to estimate the damage rate $\dot{D}(t) \equiv \frac{dD(t)}{dt}$ in terms of the so-called elastic damage rate $\dot{D}_e(t) \equiv \frac{dD_e(t)}{dt}$ and plastic damage rate $\dot{D}_p(t) \equiv \frac{dD_p(t)}{dt}$ as follows:

$$\dot{D}_e(t) = \begin{cases} 2\frac{\partial}{\partial\sigma}\left(\left(\frac{\sigma-\sigma_r}{2(\sigma'_f-\sigma_m)}\right)^{-\frac{1}{b}}\right)\frac{d\sigma}{dt} & \text{if } \sigma \geq \sigma_r \text{ and } \frac{d\sigma}{dt} \geq 0 \\ 0 & \text{Otherwise} \end{cases} \quad \ldots (6)$$

$$\dot{D}_p(t) = \begin{cases} 2\frac{\partial}{\partial\sigma}\left(\frac{1}{\varepsilon'_f}\left(\frac{\sigma-\sigma_r}{2K'}\right)^{\frac{1}{n'}}\left(1-\frac{\sigma_m}{\sigma'_f}\right)^{-\frac{c}{b}}\right)\frac{d\sigma}{dt} & \text{if } \sigma \geq \sigma_r \text{ and } \frac{d\sigma}{dt} \geq 0 \\ 0 & \text{Otherwise} \end{cases} \quad \ldots (7)$$

$$\dot{D}(t) = \left(\frac{\frac{\sigma-\sigma_r}{2E}}{\frac{\sigma-\sigma_r}{2E}+\left(\frac{\sigma-\sigma_r}{2K'}\right)^{\frac{1}{n'}}}\right)\dot{D}_e(t) + \left(\frac{\left(\frac{\sigma-\sigma_r}{2K'}\right)^{\frac{1}{n'}}}{\frac{\sigma-\sigma_r}{2E}+\left(\frac{\sigma-\sigma_r}{2K'}\right)^{\frac{1}{n'}}}\right)\dot{D}_p(t) \quad \ldots (8)$$

where $t$ indicates the *continuous* time and $\sigma(t)$ is the tensile stress at time $t$; $\sigma_m(t)$ is the mean stress of the previous cycle relative to time $t$; $\sigma_r(t)$ is reference stress at the starting point of a stress reversal cycle relative to time $t$ and is determined by rain flow cycle counting method[16]. The material parameters, $b$, $c$, $E$, $K'$, $n'$, $\varepsilon'_f$ and $\sigma'_f$, are listed in Table 1.

Remark: Equations (6) to (8) provide a conservative estimate of the instantaneous damage rate when the LEC attempts to reduce peak stresses.

Remark: If the damage rate Equation (8) is integrated over the tenure of a stress cycle, the result is the damage increment in one stress cycle. Hence, for a given profile of stress peaks and valleys, the damage rate is directly proportional to the frequency of blade vibration.

Remark: For the current application it will be seen later that the damage mitigation is derived by reducing the mean stress on the turbine blades. Note that if the damage rate Equation (8) is integrated over the tenure of a stress cycle, the result is the damage increment in one stress cycle.

| Description | Values |
|---|---|
| Fatigue strength exponent ($b$) | –0·886 |
| Fatigue ductility exponent ($c$) | –0·662 |
| Young's Modulus (E) | 193,500MPa |
| Cyclic strength coefficient ($K'$) | 1,890MPa |
| Cyclic strength hardening coefficient ($n'$) | 0·118 |
| Fatigue Ductility Coefficient ($\varepsilon'_f$) | 0·706 |
| Fatigue Strength Coefficient ($\sigma'_f$) | 1,880MPa |
| Cyclic Yield Strength ($\sigma'_y$) | 905MPa |
| Monotonic Yield Strength ($\sigma_y$) | 1,374MPa |

**Table 1**
**Properties of the turbine blade material**

### 3.3 Design of the nonlinear damage controller

The outer damage control loop in Fig. 2 is a cascaded combination of a structural model, a nonlinear fatigue damage model for the turbine blades, and a linear dynamic filter acting as the damage controller. The parameters of the dynamic filter are optimised to reduce the damage rate and accumulation at the critical points (i.e., fuel and oxidiser turbine blades) specifically under transient operations where the time-dependent load on the stressed structure is controllable. The nonlinear damage model is a simplified representation of the material behaviour so that it can be incorporated in the outer control loop for real-time execution.

The discrete-time linear damage controller is designed by identification of the elements of its A, B, C, and D matrices. The state-space model needs to be structured in canonical forms to reduce the number of design parameters to be optimised. One option is to have a diagonal A matrix with distinct real diagonal elements is equivalent to constraining the damage controller to have distinct real eigenvalues. Repeated and/or pair wise complex poles can be included at the expense of computational complexity. For a damage controller with $m$ inputs, $p$ outputs, and $n$ states, the number of parameters to be optimised is: n (for the diagonal $n \leftrightarrow n$ A-matrix) + $n\,m$ (for the $n \leftrightarrow m$ B matrix) + $p\,n$ (for the $p \leftrightarrow n$ C matrix) + $p\,m$ (for the $p \leftrightarrow m$ D matrix) = $(p + m + 1)\,n + p\,m$ parameters.

The parameters of the linear dynamic filter are identified by minimising a cost functional using nonlinear optimisation. For each evaluation of the cost functional, a nominal computer simulation needs to be performed. As the value of the cost functional is obtained from the results of this simulation, the simulation results are a function of the current damage controller chosen by the optimisation routine. Since damage controllers designed using this method are directly based on the manoeuvre used in the optimisation process, such manoeuvres should be chosen to be broadly representative of all plant operation. The resulting damage controller is then validated by examining the results of various other typical manoeuvres that the plant is expected to perform with this damage controller in the damage feedback loop.

The cost functional includes the effects of both reference signal tracking performance and damage in the turbine blades:

$$J^{tot} = J^{perf} + J^{dam} \quad \ldots (9)$$

The performance part of the cost functional ($J^{perf}$) is composed of penalties on:

($i$) Tracking error of the main thrust chamber hot gas pressure (in units of psi):

$$J_{press} = \sum_{k=1}^{N-1} Q_{press}\left(\frac{y_{press}(kT) - y^{ref}_{press}(kT)}{y^{ref}_{press}(kT) + 1{\cdot}0}\right)^2 \quad \ldots (10)$$

$$J^{ss}_{press} = Q^{ss}_{press}\left(\frac{y_{press}(NT) - y^{ref}_{press}(NT)}{y^{ref}_{press}(NT) + 1{\cdot}0}\right)^2 \quad \ldots(11)$$

(ii) Tracking error of the $O_2/H_2$ mixture ratio:

$$J_{O_2/H_2} = \sum_{k=1}^{N-1} Q_{O_2/H_2}\, g(kT) \quad \ldots(12)$$

where

$$g(kT) = \begin{cases} \left(\dfrac{y_{O_2/H_2}(kT) - 6{\cdot}02}{6{\cdot}02 + 1{\cdot}0}\right)^2 & \text{if } y_{O_2/H_2}(kT) \geq 6{\cdot}04 \\ 0 & \text{otherwise} \end{cases} \quad \ldots(13)$$

and

$$J^{ss}_{O_2/H_2} = Q^{ss}_{O_2/H_2}\left(\frac{y_{O_2/H_2}(NT) - 6{\cdot}02}{6{\cdot}02 + 1{\cdot}0}\right)^2 \quad \ldots(14)$$

The fatigue damage part of the cost functional ($J^{dam}$) is composed of penalties on:
(*i*) Damage rate in the $O_2$ turbine blades:

$$J_{\dot{D}_{O_2}} = \sum_{k=1}^{N} Q_{\dot{D}_{O_2}} \dot{D}_{O_2}(kT) \quad \ldots(15)$$

(*ii*) Damage rate in the $O_2/H_2$ turbine blades:

$$J_{\dot{D}_{H_2}} = \sum_{k=1}^{N} Q_{\dot{D}_{H_2}} \dot{D}_{H_2}(kT) \quad \ldots(16)$$

(*iii*) Accumulated damage in the $O_2$ turbine blades:

$$J_{D_{O_2}} = Q_{D_{O_2}}\left(D_{O_2}(NT) - D_{O_2}(0T)\right) \quad \ldots(17)$$

(*iv*) Accumulated damage in the $H_2$ turbine blades:

$$J_{D_{H_2}} = Q_{D_{H_2}}\left(D_{H_2}(NT) - D_{H_2}(0T)\right) \quad \ldots(18)$$

Both the pressure and $O_2/H_2$ ratio components of the cost functional have extra weight on the error at the final sampling instant (i.e. the N[th] sample). Adjusting these extra weights is a means to control the steady state behaviour of the simulation. Increasing the steady-state weights, $Q^{ss}_{press}$ and/or $Q^{ss}_{O_2/H_2}$ tend to decrease the settling time of the control system. Also, since it is desired to keep the mixture ratio below a value of 6·04 during the transient, the $O_2/H_2$ xture ratio is penalised only if it exceeds 6·04 for samples 1 to .–1. The final, Nth, sample of the $O_2/H_2$ ratio is penalised whether its value is above or below 6·04, since it is necessary for the $O_2/H_2$ ratio to reach 6·02 in the steady state. The factor of 1·0 added in the denominator of Equations (10), (11), (13) and (14) is a convenient way to combine the features of absolute and relative error and is often used in practice[18].

The accumulated damage and damage rate components of the cost functional do not contain an absolute value operator or squared terms because damage rate and accumulation are always positive. In the accumulated damage components (Equations (17) and (18)), the initial accumulated damage is subtracted from the final damage at time 0·6 seconds to penalise the damage accumulated during the manoeuvre.

Since the governing equations and the cost functional are nonlinear in nature, a nonlinear programming technique is used to identify the optimal parameters of the damage controller. Also, in order to evaluate the cost functional, a time consuming simulation must be performed. Therefore, a nonlinear programming technique known as sequential quadratic programming (SQP) is employed, which has the reputation of being able to efficiently and successfully solve a wide range of nonlinear programming problems in which the evaluation of the cost functional is a computationally intensive procedure. An SQP Fortran Software package developed by Gill *et al*[18] at Stanford University called NPSOL is utilised to design the damage controller.

## 4.0 SIMULATION RESULTS AND DISCUSSION

The design of the damage controller is based on the upthrust transients of the rocket engine. This operating condition is represented in Fig. 4 by a ramp-up simulation of the hot gas pressure in the main thrust chamber from 2,700psi (18·62MPa) to 3,000psi (20·69MPa) at a rate of 3,000psi/sec (20·69MPa/sec), followed by a steady state at the final 3,000 psi (20·69MPa) pressure for 500ms. The $O_2/H_2$ mixture ratio for this simulation scenario is kept at a constant value of 6·02. After each simulation run, the generated data are sent to the cost functional subroutine. The data set consists of samples of the chamber pressure, the $O_2/H_2$ mixture ratio, the damage rate in the $O_2$ turbine blade, and the damage rate in the $H_2$ turbine blade. Since the duration of the simulation is 0·6 seconds and each trajectory is sampled every two milliseconds, there is a total of $N = 300$ samples sent to the cost functional subroutine for each of the four trajectories listed above. In addition, the value of accumulated damage for the $O_2$ and $H_2$ turbines at time $t = 0{\cdot}6$ seconds is also used for the calculation of the value of the cost functional.

The initial fatigue damage for both the $O_2$ and $H_2$ turbine blades is assumed to be $D(0) = 0{\cdot}1$. The following set of weights in Equations (10) to (18) are found to produce an acceptable damage controller:

$$Q_{press} = 21{\cdot}0 \qquad Q_{\dot{D}_{O_2}} = 719{\cdot}42$$

$$Q^{ss}_{press} = 10^6 \qquad Q_{\dot{D}_{H_2}} = 5{\cdot}31\times10^4$$

$$Q_{O_2/H_2} = 2{\cdot}6\times10^8 \qquad Q_{D_{O_2}} = 3{\cdot}60\times10^5$$

$$Q^{ss}_{O_2/H_2} = 2{\cdot}6\times10^8 \qquad Q_{D_{H_2}} = 2{\cdot}66\times10^7$$

For the rocket engine under consideration, the damage controller is designed using 15 states ($n = 15$), two actuator inputs ($m = 2$), and

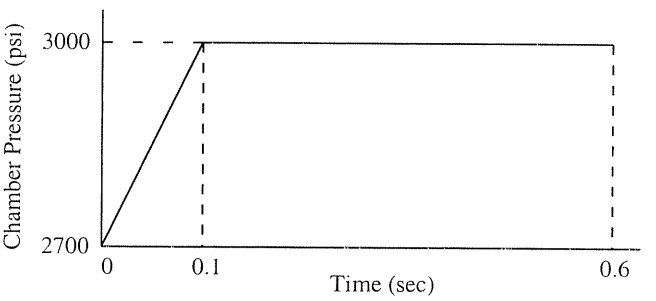


Figure 4. Reference trajectory for chamber pressure.

two sensor outputs ($p = 2$). Therefore, the number of parameters to be optimised is $(n \times (1 + m + p) + m \times p) = 79$. It is found that, after designing the 15-state damage controller, reducing the number of controller states to five via Hankel model order reduction does not significantly change the input/output characteristics of the controller. Therefore, the results that follow are created by using the five-state reduced order damage controller. This implies that it is more efficient to directly optimise a controller with five states instead of 15 states. Unfortunately, it is not known how to optimally choose the number of controller states *a priori*.

The damage controller is designed based on simulated transient trajectories of engine performance variables and damage in $O_2$ and $H_2$ turbine blades when the chamber pressure is raised from 2,700psi to 3,000psi. Each plot displays two cases: (*i*) no damage control (i.e. $u(k) = u^{ff}(k) + u^{fb}(k)$); and (*ii*) with damage control (i.e. $u(k) = u^{ff}(k) + u^{fb}(k) + u^{dam}(k)$). The transient trajectories of chamber pressure and $O_2/H_2$ ratio for the two cases are compared in Fig. 5. The damage controller causes a slower rise time, a longer settling time, and less overshoot in the chamber pressure transient. The damage controller also causes the $O_2/H_2$ ratio to deviate farther from the desired value of 6·02 than the case with no damage control. However, the mixture ratio settles to 6·02 at steady state and remains within acceptable bounds throughout the duration of the simulation for both cases. The damage rate and accumulation plots of the $O_2$ and $H_2$ turbine blades for the first one second of the 2,700psi (18·62MPa) to 3,000psi (20·69MPa) simulation are shown in Figs 6 and 7. Table 2 summarises the accumulated damage after this time interval for the two simulation cases (i.e., with and without damage control) for the two turbine blades.

The quality of the control designed above is now tested on a transient manoeuvre which takes the chamber pressure from 2,100psi (14·48MPa) to 3,000psi at a rate of 3,000psi/sec. This manoeuvre involves a larger pressure increase than the nominal manoeuvre used to design the damage controller, and therefore is expected to produce a larger amount of damage accumulation. The chamber pressure and $O_2/H_2$ ratio trajectories with and without the damage controller are shown in Fig. 8. As in the 2,700psi (18·62MPa) to 3,000psi (20·69MPa) case, the damage controller acts to 'slow down' the transient as it approaches the final pressure of 3,000psi (20·69MPa). Although the damage controller causes the $O_2/H_2$ ratio to deviate from the desired value of 6·02 more than it did during the 2,700psi (18·62MPa) to 3,000psi (20·69MPa) simulation, it settles to 6·02 at steady state and remains within acceptable bounds throughout the simulation. The mixture ratio is important in this application as an indicator of chamber temperature as well as propellant utilisation. The damage rate and accumulation plots for the first 1·2

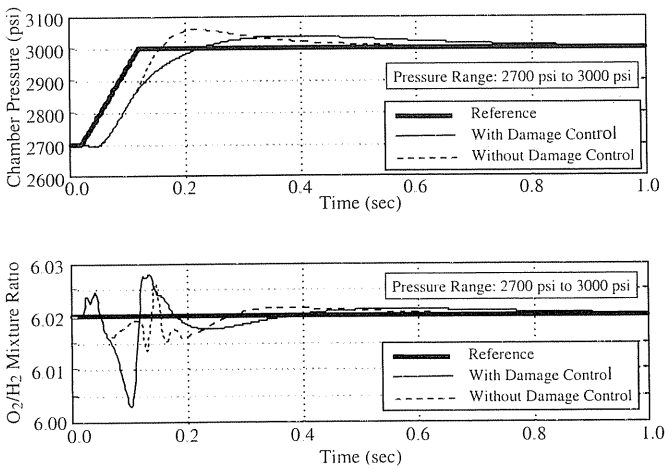


Figure 5. Transients of engine performance variables (2,700psi – 3,000psi).

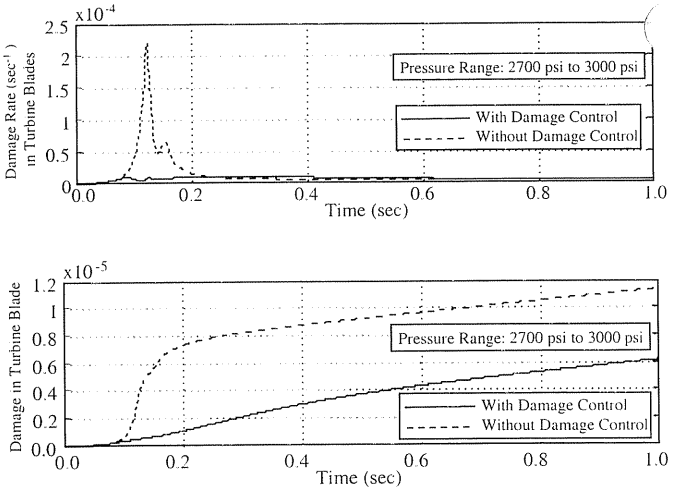


Figure 6. Damage in hydrogen turbine blades (2,700psi – 3,000psi).

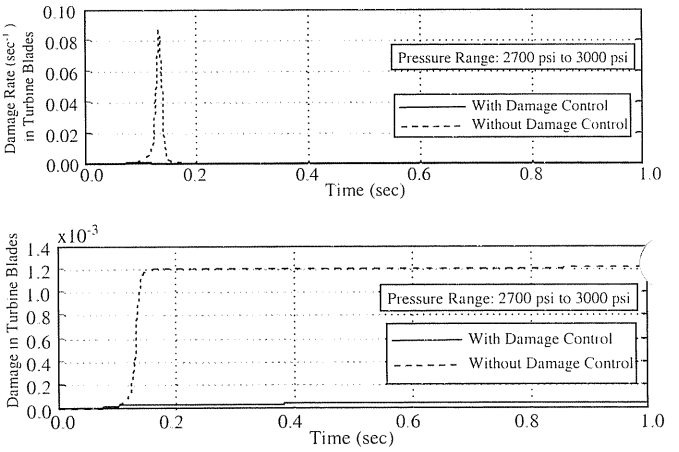


Figure 7. Damage in oxygen turbine blades (2,700psi – 3,000psi).

seconds of the 2,100psi (14·48MPa) to 3,000psi simulation are shown in Figs 9 and 10. Table 3 summarises the accumulated damage for this transient.

## 5.0 SUMMARY AND CONCLUSIONS

The key concept of life extending control (LEC), as presented in this paper, is to separate the design of the linear performance controller from the nonlinear damage controller. A two-tier architecture has been proposed for the LEC system that consists of a linear performance controller in the inner loop and a nonlinear damage controller in the outer loop. The robust high performance controller in the inner loop is designed using standard (linear) techniques to achieve an acceptable dynamic response for a reusable rocket engine which is similar to the SSME. The combination of rocket engine dynamics and the linear controller in the inner loop becomes the augmented plant for design of the nonlinear damage controller (in the outer loop) that is a cascaded combination of a (static) nonlinear character-

**Table 2**
**Accumulated damage (after one sec) for 2,700psi - 3,000psi simulation**

| | Without damage control | With damage control | Ratio |
|---|---|---|---|
| $H_2$ blades | $1{\cdot}13 \times 10^{-5}$ | $6{\cdot}15 \times 10^{-6}$ | 1·8 |
| $O_2$ blades | $1{\cdot}21 \times 10^{-3}$ | $3{\cdot}45 \times 10^{-5}$ | 35·1 |

| | Without damage control | With damage control | Ratio |
|---|---|---|---|
| $_2$ blades | $2{\cdot}46 \times 10^{-5}$ | $9{\cdot}61 \times 10^{-6}$ | 2·6 |
| $_2$ blades | $2{\cdot}48 \times 10^{-3}$ | $7{\cdot}01 \times 10^{-5}$ | 35·4 |

**Table 3**
**Accumulated damage (after 1·2 sec) for 2,100psi - 3,000psi simulation**

isation of fatigue damage rate in the turbine blades and a linear dynamic filter. Parameters of the filter are optimised to reduce the damage rate and accumulation at the critical points (i.e. fuel and oxidiser turbine blades) specifically under transient operations in which the time-dependent load on the stressed structure is controllable. Damage modelling is a critically important aspect of life-extending control (LEC). The objective of this paper is to establish a viable design method for LEC systems that take the nonlinear damage characteristics of structural materials into account. Benefits of this controller design approach are: (*i*) The controller parameter identification in the two individual loops is decoupled and can be carried out by standard commercially available software; and (*ii*) There is no need to determine a feedforward control sequence which is sensitive to plant modelling uncertainties and variations in the initial conditions; (*iii*) The design methodology allows adaptation of the damage controller part of the LEC module to augment a conventional performance controller of a rocket engine.

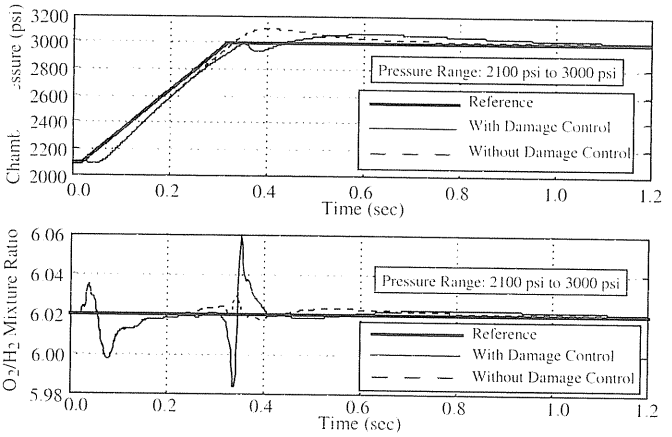


Figure 8. Transients of engine performance variables (2,100psi - 3,000psi).

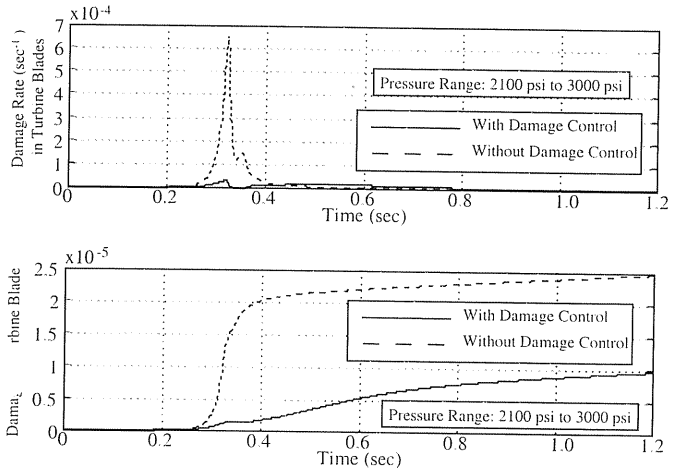


Figure 9. Damage in hydrogen turbine blades (2,100psi - 3,000psi).

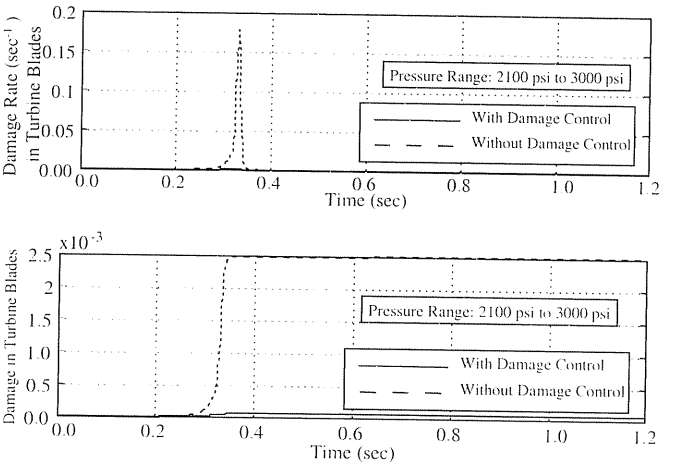


Figure 10. Damage in oxygen turbine blades (2,100 psi - 3,000psi).

## ACKNOWLEDGEMENTS

The research work reported in this paper has been supported in part by: NASA Glenn Research Center under Grant No NAG 3-2016, National Science Foundation under Grant No CMS-9819074; National Academy of Sciences under a Research Fellowship award to the first author.

## REFERENCES

1. DAI, X. and RAY, A. Damage-mitigating control of a reusable rocket engine: Parts I and II, *ASME J of Dyn Sys, Measur and Ctrl*, 1996, **118**, (3), pp 401-415.
2. RAY, A. and CAPLIN, J. Damage mitigating control of aircraft: trade-off between flight performance and structural durability, *Aeronaut J*, 2000, 104, (1039), pp 397-408.
3. RAY, A. and DAI, X. Damage-mitigating control of a reusable rocket engine, 1995, NASA Contractor Report 4640 under Lewis Research Center Grant NAG 3-1240.
4. LORENZO, C.F. and MERRILL, W.C. An intelligent control system for rocket engines: need, vision, and issues, *Control Systems Magazine*, **12,** (1), 1991, pp 42-46.
5. RAY, A., WU, M.K., CARPINO, M. and Lorenzo, C.F. Damage-mitigating control of mechanical systems: Parts I and II, *ASME J of Dyn Sys, Measur and Ctrl*, 1994, **116,** (3), pp 437-455.
6. HOLMES, M. and RAY, A. Fuzzy damage mitigating control of mechanical structures, *ASME J of Dyn Sys, Measur and Ctrl*, 1998, **120,** (2), pp 249-256.
7. ROZAK, J.H. and RAY, A. Robust multivariable control of rotorcraft in forward flight, *J of the Ameri Heli Soc*, 1997, **42,** (2), pp 149-160.
8. ROZAK, J.H.,and RAY, A. Robust multivariable control of rotorcraft in forward flight: impact of bandwidth on fatigue life, *J of the Ameri Heli Soc*, 1998, **43,** (3), pp 195-201.
9. KALLAPPA, P., HOLMES, M.S. and RAY, A. Life extending control of fossil power plants for structural durability and performance enhancement, *Automatica*, 1997, pp 1101-1118.
10. KALLAPPA, P. and RAY, A. Fuzzy wide-range control of fossil power plants for life extension and robust performance, *Automatica*, 2000, **36**, (1), pp 69-82.
11. ZHANG, H. and RAY, A. Robust damage-mitigating control of mechanical structures: experimental validation on a test apparatus, *ASME J of Dyn Sys, Measur and Ctrl*, 1999, **121**, (3), pp 377-385.
12. ZHOU, K., DOYLE, J.C. and GLOVER, K. *Robust and Optimal Control*, 1996, Prentice-Hall.
13. BAMIEH, B.A. and PEARSON, J.B. A general framework for linear periodic systems with applications to $H_\infty$ sampled-data control, *IEEE Transactions on Automatic Control*, 1992, **37,** (4), pp 418-435.
14. SIVASHANKAR, N. and KHARGONEKAR, P.P. Robust stability and performance analysis of sampled-data systems, *IEEE Transactions on Automatic Control*, 1993, **38,** (1), pp 58-69.

15. BALAS, G.J., DOYLE, J.C., GLOVER, K., PACKARD, A. and SMITH, R. μ-Analysis and synthesis toolbox, MUSYN and The Math Works, 1993.
16. SURESH, S. *Fatigue of Materials,* 1991, Cambridge University Press, Cambridge, UK.
17. NEWMAN, J.C. *FASTRAN-II – A fatigue crack growth structural analysis program,* 1992, NASA Technical Memorandum 104159, Langley Research Center, Hampton, VA.
18. GILL, P.E., MURRAY, W., SAUNDERS, M.A. and WRIGHT, M.H. *User's Guide for NPSOL (Version 4·0): A Fortran Package for Nonlinear Programming,* 1986, Stanford Office of Technology Licensing, 350 Cambridge Avenue, Suite 250, Palo Alto, California 94306.